JOURNAL OF COMPUTATIONAL PHYSICS 70, 182–192 (1987)

Numerical Solutions for the Pressure Poisson Equation with Neumann Boundary Conditions Using a Non-staggered Grid, I

S. ABDALLAH

Applied Research Laboratory, The Pennsylvania State University, P.O. Box 30, State College, Pennsylvania 16804

Received November 11, 1985; revised August 4, 1986

Numerical solutions are obtained for the pressure Poisson equation with Neumann boundary conditions using a non-staggered grid. The existence of a solution for this equation requires the satisfaction of a compatibility condition which relates the source of the Poisson equation and the Neumann boundary conditions. This compatibility condition is not automatically satisfied on non-staggered grids. Failure to satisfy the compatibility condition leads to non-convergent iterative solutions. Consistent finite-difference approximations for the pressure equation with Neumann boundary conditions are developed to satisfy the compatibility condition on non-staggered grids. The method is applied to calculate the pressure coefficient in a driven cavity when given the velocity field. The velocity is computed from the stream function–vorticity formulation of the Navier–Stokes equations. © 1987 Academic Press, Inc.

INTRODUCTION

Owing to errors in the numerical approximations, direct integration of the momentum equation to calculate the pressure of incompressible flow gives different results when different paths are used to get to the same point [1]. A more accurate solution [1] for the pressure is obtained from a Poisson equation (divergence of the momentum equation) with Neumann boundary conditions. Solutions for the Poisson equation with Neumann boundary conditions exist only if a compatibility condition is satisfied. This condition relates the source of the Poisson equation and the Neumann boundary conditions (Green's theorem). This compatibility condition is not automatically satisfied on non-staggered grids. Failure to satisfy the compatibility condition leads to non-convergent iterative solutions [1–6]. Two remedies were suggested by Briley [4] and Miyakoda [5] to satisfy the compatibility condition. Briley [4] modified the source of the Poisson equation in order to meet this condition. While Miyakoda recommended in Ref. [5] that the boundary conditions be incorporated directly into the finite-difference scheme at interior points adjacent to the boundaries. The use of these remedies improves the convergence of the numerical solutions for the Poisson equation, however, the pressure problem remains a major difficulty [1–6].

0021-9991/87 $3.00

This paper presents a new method for the solution of the pressure Poisson equation with Neumann boundary conditions on non-staggered grids. Consistent finite-difference approximations for the pressure equation with Neumann boundary conditions are developed to exactly satisfy the compatibility condition. Details of the analysis are given in the following sections.

MATHEMATICAL FORMULATION

In this section, the pressure Poisson equation of incompressible flow is derived from the divergence of the momentum equation. For clarity, the analysis is developed for the two-dimensional case; however, it is applicable without modification for three dimensions.

Governing Equations

The x-momentum equation is

$$v\omega = P_x + \frac{1}{\text{Re}}\,\omega_y. \tag{1}$$

The y-momentum equation is

$$-u\omega = P_y - \frac{1}{\text{Re}}\,\omega_x, \tag{2}$$

where

$$\omega = v_x - u_y. \tag{3}$$

Equations (1) and (2) are written in terms of the vorticity ω for reasons that will be explained later in the consistent finite-difference approximation section. In the above equations, P, ω, u, and v are the total pressure, vorticity, velocity component in the x-direction, and velocity component in the y-direction, respectively. Re is the Reynolds number.

Differentiating Eq. (1) with respect to x and Eq. (2) with respect to y and adding, one obtains

$$P_{xx} + P_{yy} = \sigma, \tag{4}$$

where

$$\sigma = (v\omega)_x - (u\omega)_y. \tag{4a}$$

The subscripts x and y in all the governing equations refer to partial derivatives with respect to x and y, respectively. Equation (4) is a second order elliptic partial differential equation of the Poisson type. It is explicitly independent of the Reynolds number because the diffusion terms are eliminated by the continuity equation.

Boundary Conditions

Referring to Fig. 1, the following Neumann boundary conditions are obtained by applying the momentum equations (1) and (2) at the solid boundaries:

$$P_x = v\omega - \frac{1}{\mathrm{Re}}\,\omega_y \qquad \text{at } x = 0, 1 \tag{5a}$$

and

$$P_y = -u\omega + \frac{1}{\mathrm{Re}}\,\omega_x \qquad \text{at } y = 0, 1. \tag{5b}$$

Solutions to Eq. (4) with the Neumann boundary conditions (5) are unique within an arbitrary constant. This arbitrary constant can be determined by using the relation

$$\int_{y=0}^{1} \int_{x=0}^{1} p\, dx\, dy = \text{constant}. \tag{6}$$

Compatibility Condition

The existence of a solution for Eq. (4) with the Neumann boundary conditions (5) requires the satisfaction of the integral relation

$$\int_{y=0}^{1} \int_{x=0}^{1} \sigma\, dx\, dy = \int P_n\, dS, \tag{7}$$

where n is the outward normal to the boundary contour S, enclosing the solution domain (see Fig. 1).

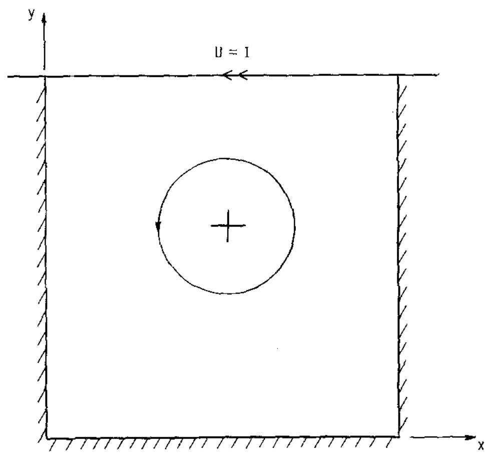

FIG. 1. Cavity geometry.

Equation (7) is a consequence of Green's theorem. Failure to satisfy this condition causes the iterative solutions to drift slowly and endlessly [1]. In the following sections it is shown that the compatibility condition (7) is not automatically satisfied on a non-staggered grid.

With reference to Fig. 2, the Poisson equation (4) and the boundary conditions (5) are approximated on a non-staggered grid with grid increments h in both the x- and y-directions. All partial derivatives in Eqs. (4) and (5) are approximated using second order accurate formulas.

Finite-Difference Approximation for Eq. (4)

$$\begin{aligned} &P_{i+1,j}+P_{i-1,j}+P_{i,j+1}+P_{i,j-1}-4P_{i,j} \\ &\quad=[(v\omega)_{i+1,j}-(v\omega)_{i-1,j}-(u\omega)_{i,j+1}+(u\omega)_{i,j-1}]\,h/2 \\ &\quad(2\leqslant i\leqslant M-1;\ 2\leqslant j\leqslant N-1). \end{aligned} \tag{8}$$

Finite-Difference Approximation for Eq. (5)

$$P_{2,j}-P_{1,j}=-(\omega_{1,j+1}-\omega_{1,j-1})/2\text{Re} \qquad (2\leqslant j\leqslant N-1) \tag{9a}$$

$$-P_{M,j}+P_{M-1,j}=(\omega_{M,j+1}-\omega_{M,j-1})/2\text{Re} \qquad (2\leqslant j\leqslant N-1) \tag{9b}$$

$$P_{i,2}-P_{i,1}=(\omega_{i+1,1}-\omega_{i-1,1})/\text{Re} \qquad (2\leqslant i\leqslant M-1) \tag{9c}$$

$$-P_{i,N}+P_{i,N-1}=h(u\omega)_{i,N}-(\omega_{i+1,N}-\omega_{i-1,N})/2\text{Re} \qquad (2\leqslant i\leqslant M-1), \tag{9d}$$

where M and N are the number of grid points in the x- and y-directions, respectively.

The summation of the left- and right-hand members (LHM and RHM) of Eqs. (8) and (9) can be interpreted as the divergence theorem in discrete form [6],

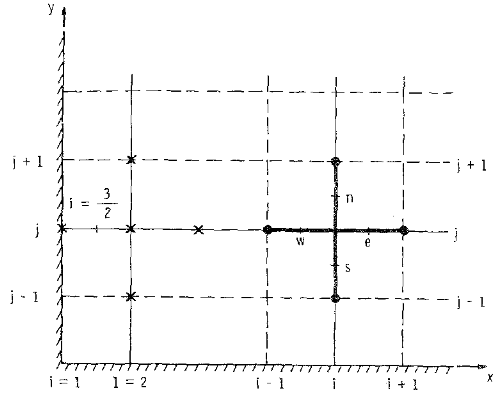

FIG. 2. Finite-difference grid.

$$\text{LHM} = 0 \tag{10a}$$

$$\text{RHM} = \left\{ \sum_{i=2}^{M-1} [(u\omega)_{i,2} - (u\omega)_{i,N-1} + (u\omega)_{i,N}] + \sum_{j=2}^{N-1} [(v\omega)_{M-1,j} - (v\omega)_{2,j}] \right\} h/2$$
$$+ (\omega_{1,2} - \omega_{1,N-1} + \omega_{M,N-1} - \omega_{M,2}$$
$$+ \omega_{M-1,1} - \omega_{2,1} + \omega_{2,N} - \omega_{M-1,N})/2\text{Re}. \tag{10b}$$

It is clear from Eqs. (10a) and (10b) that the compatibility condition (7) is not obviously satisfied on non-staggered grids.

Consistent Finite-Difference Approximations

In the present study, the compatibility condition (7) is exactly satisfied on a non-staggered grid. This is done by using consistent finite-difference approximations for the source, σ, and the Neumann boundary conditions, P_n. First, Eq. (4) is rewritten in a divergence form

$$(P_x - v\omega)_x + (P_y + u\omega)_y = 0. \tag{11}$$

Referring to Fig. 2, Eq. (11) is approximated at the grid point (i, j) using second order accurate formulas.

$$(P_x - v\omega)_\text{e} - (P_x - v\omega)_\text{w} + (P_y + u\omega)_\text{n} - (P_y + u\omega)_\text{s} = 0. \tag{12}$$

The pressure gradients P_x and P_y in Eq. (12) are approximated using second order accurate formulas at the locations e, w, n, and s as

$$(P_x)_\text{w} = (P_{i,j} - P_{i-1,j})/h \tag{13a}$$
$$(P_x)_\text{e} = (P_{i+1,j} - P_{i,j})/h \tag{13b}$$
$$(P_y)_\text{s} = (P_{i,j} - P_{i,j-1})/h \tag{13c}$$
$$(P_y)_\text{n} = (P_{i,j+1} - P_{i,j})/h. \tag{13d}$$

The terms $(v\omega)$ and $(u\omega)$ at the locations (e, w) and (n, s) are calculated from their values at the grid locations by averaging as

$$(v\omega)_\text{w} = (v_{i,j} + v_{i-1,j})(\omega_{i,j} + \omega_{i-1,j})/4 \tag{14a}$$
$$(v\omega)_\text{e} = (v_{i+1,j} + v_{i,j})(\omega_{i+1,j} + \omega_{i,j})/4 \tag{14b}$$
$$(u\omega)_\text{s} = (u_{i,j} + u_{i,j-1})(\omega_{i,j} + \omega_{i,j-1})/4 \tag{14c}$$
$$(u\omega)_\text{n} = (u_{i,j+1} + u_{i,j})(\omega_{i,j+1} + \omega_{i,j})/4. \tag{14d}$$

Substituting Eqs. (13) and (14) in Eq. (12), one obtains

$$\begin{aligned} &P_{i+1,j}+P_{i-1,j}+P_{i,j+1}+P_{i,j-1}-4P_{i,j} \\ &\quad=[(v_{i+1,j}+v_{i,j})(\omega_{i+1,j}+\omega_{i,j})-(v_{i,j}+v_{i-1,j})(\omega_{i,j}+\omega_{i-1,j}) \\ &\qquad-(u_{i,j+1}+u_{i,j})(\omega_{i,j+1}+\omega_{i,j})+(u_{i,j}+u_{i,j-1})(\omega_{i,j}+\omega_{i,j-1})]\, h/4. \end{aligned} \tag{15}$$

Equation (15) is solved for P at all the interior points ($2 \leqslant i \leqslant M-1$ and $2 \leqslant j \leqslant N-1$). When Eq. (11) is applied at the grid points next to the boundaries, for example, at $i=2$, the pressure gradient $(P_x)_w$ is evaluated at the location $x=h/2$. For consistency, the pressure gradient P_x computed from the boundary condition (5a) should be evaluated at the location $x=h/2$ and not at $x=0$. The evaluation of the Neumann boundary conditions (5) at the boundaries as was done in Eq. (9) is inconsistent with Eq. (11) when applied at the grid points adjacent to the boundaries. This is one reason that the compatibility condition (7) is not satisfied on non-staggered grids.

Using second order accurate formulas, the derivative boundary condition Eq. (5a) is evaluated at $x=h/2$ as

$$\begin{aligned} P_{2,j}-P_{1,j}=&-(\omega_{2,j+1}+\omega_{1,j+1}-\omega_{2,j-1}-\omega_{1,j-1})/4R_e \\ &+v_{2,j}(\omega_{2,j}+\omega_{1,j})\, h/4 \qquad (2 \leqslant j \leqslant N-1). \end{aligned} \tag{16a}$$

Similar expressions are derived using Eq. (5) at $x=1-h/2$, $y=h/2$, and $y=1-h/2$ in Eqs. (16b)–(16d), respectively.

$$\begin{aligned} -P_{M,j}+P_{M-1,j}=&(\omega_{M,j+1}+\omega_{M-1,j+1}-\omega_{M,j-1}-\omega_{M-1,j-1})/4R_e \\ &-v_{M-1,j}(\omega_{M,j}+\omega_{M-1,j})\, h/4 \qquad (2 \leqslant j \leqslant N-1) \end{aligned} \tag{16b}$$

$$\begin{aligned} P_{i,2}-P_{i,1}=&(\omega_{i+1,2}+\omega_{i+1,1}-\omega_{i-1,2}-\omega_{i-1,1})/4R_e \\ &-u_{i,2}(\omega_{i,2}+\omega_{i,1})\, h/4 \qquad (2 \leqslant i \leqslant M-1) \end{aligned} \tag{16c}$$

$$\begin{aligned} -P_{i,N}+P_{i,N-1}=&-(\omega_{i+1,N}+\omega_{i+1,N-1}-\omega_{i-1,N}-\omega_{i-1,N-1})/4R_e \\ &+(u_{i,N}+u_{i,N-1})(\omega_{i,N}+\omega_{i,N-1})\, h/4 \qquad (2 \leqslant i \leqslant M-1). \end{aligned} \tag{16d}$$

The summation of the left- and right-hand members of Eqs. (15) and (16) in this case gives

$$\text{LHM}=0$$

$$\text{RHM}=0.$$

This proves that the compatibility condition (7) is *exactly* satisfied in discrete form on a non-staggered grid.

It is important to mention here that the viscous terms in the momentum equations (1) and (2) do not appear in the source of the pressure equation (4);

however, they are in the Neumann boundary conditions (5). In order to satisfy the compatibility condition (7), the integral of the viscous terms over the boundary contour should cancel. This can be achieved by writing the viscous terms as the curl of the vorticity vector in Eqs. (1) and (2). This is the second reason that the compatibility condition (7) is not satisfied on non-staggered grids. Although the convection terms in the momentum equations (1) and (2) are also written in terms of the vorticity, ω, this is not necessary in the present analysis.

Calculation of the Velocity Field

In order to solve Eqs. (4) and (5) for the pressure, the velocity field is first computed from the momentum equations (1) and (2) and the continuity equation.

Equations (1), (2) and continuity are solved here to second order accuracy using the well-known stream function–vorticity formulation [7].

NUMERICAL RESULTS

Numerical solutions for the stream function and vorticity equations are obtained using the successive over-relaxation (SOR) method [7]. After the velocity field is calculated from the solution of the stream function, the pressure is obtained from the solution of Eq. (15) using the SOR method.

Numerical results are obtained for the driven cavity shown in Fig. 1 at Re = 100 using 41 × 41 grid points. The stream function and vorticity contours are compared with the numerical results of Ref. [7] in Figs. 3 and 4. It can be seen from these figures that the results of Ref. [7] are duplicated here, as they should be, because the same method is used.

Given the velocity field, the pressure Poisson equation is solved for the total pressure P. The static pressure is computed from the total pressure and the velocity using the relation $P_s = P - \frac{1}{2}(u^2 + v^2)$. The static and total pressure coefficient con-

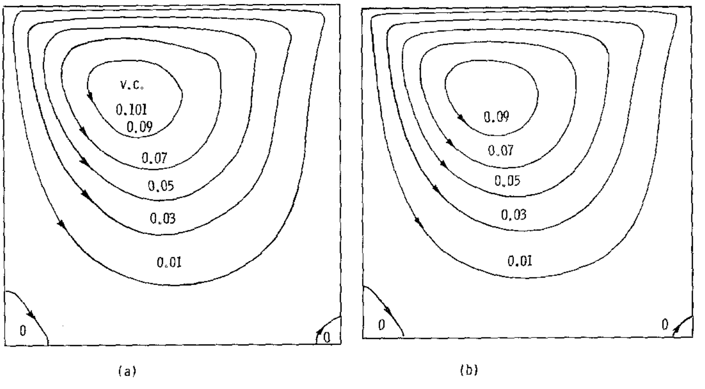

FIG. 3. Stream function contours at Re = 100. (a) Ref. [7], (b) present results.

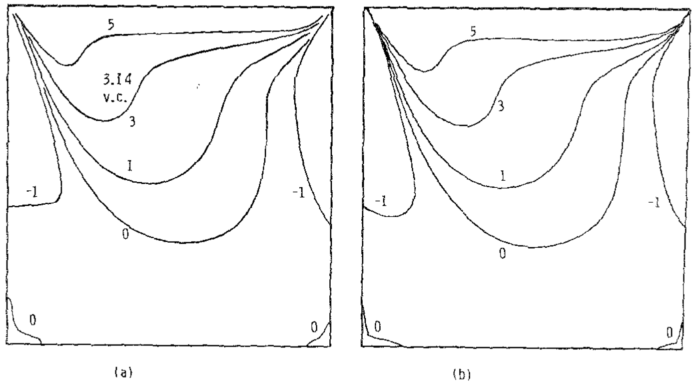

FIG. 4. Vorticity contours at Re = 100. (a) Ref. [7], (b) present results.

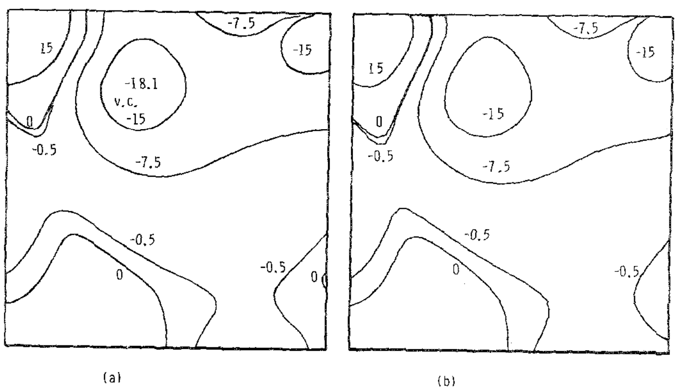

FIG. 5. Static pressure contours (Re C_{p_s}) at Re = 100. (a) Ref. [7], (b) present results.

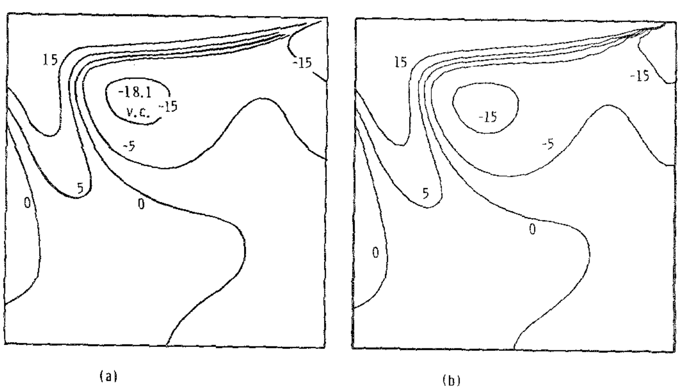

FIG. 6. Total pressure contours (Re C_{p_t}) at Re = 100. (a) Ref. [7], (b) present results.

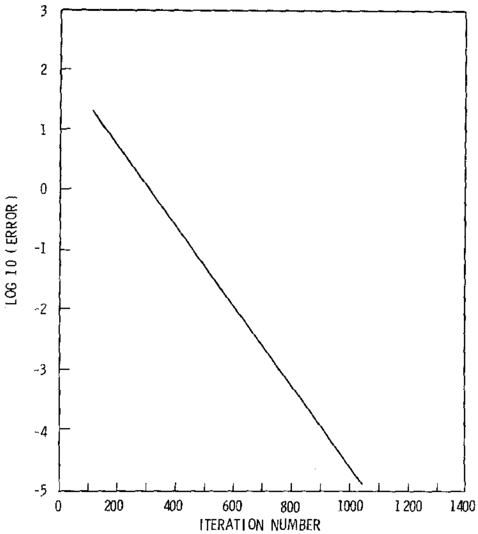

FIG. 7. Error in the pressure Poisson equation.

tours C_{p_s} and C_{p_t} are shown in Figs. 5 and 6, respectively. The pressure coefficient C_p is defined as $C_p = 2(P - P_c)/U^2$, where P_c is the pressure at the center of the cavity lower wall and U is the reference velocity. It can be seen from Figs. 5 and 6 that the computed results are in good argument with the results of Ref. [7]. Burggraf [7] computed the pressure by direct integration of the momentum equations using a fine grid. No details are given about the integration path used in these calculations. Because the Reynolds number is relatively small, the direct integration of the momentum equations should yield accurate results on a fine grid. Since, the pressure Poisson equation (4) is explicitly independent of the Reynolds number, further testing at different Reynolds numbers is unnecessary.

The convergence characteristics of the pressure Poisson equation are shown in Fig. 7. The vertical axis shows the average error at a point plotted against the number of iterations. The average error is reduced to the specified limit of 10^{-8} at iteration step 1000. All calculations are obtained using an over-relaxation factor of 1.0. No attempt was made to optimize any of the relaxation factors used in the present study.

CONCLUSIONS

A new method is developed for the numerical solution of the pressure Poisson equation with Neumann boundary conditions when the stream function–vorticity method is used to obtain the velocity field. The method exactly satisfies the compatibility condition, Eq. (7), on a non-staggered grid. It consists of three steps:

(1) Write the viscous terms in the momentum equations in terms of the vorticity.

(2) Write the Poisson equation in a conservative form (Eq. (4)).

(3) Use consistent finite-difference approximations for the Poisson equation and the Neumann boundary conditions (Eqs. (12)–(16)).

The method is tested for the driven cavity problem which is a well-documented test case. Convergence of the pressure equation is demonstrated (Fig. 7) and confirms the analytical development of the method. Both the results of Fig. 7 and the analytical proof are independent of the flow field (Reynolds number) and the geometry of the test problem.

Appendix: Nomenclature

h	grid spacing
M, N	number of grid points in x- and y-directions, respectively
P	total pressure
S	boundary contour enclosing the solution domain
u, v	velocity components in x- and y-directions, respectively
U	velocity of the cavity upper wall
C_p	pressure coefficient: $2(p-pc)/U^2$
C_{p_s}, C_{p_t}	static and total pressure coefficients, respectively
dS	increment along the boundary contour S
LHM, RHM	summation of the left- and right-hand members of the compatibility condition
P_c	pressure at the centre of the cavity lower wall
P_s	static pressure
Re	Reynolds number
σ	right-hand side of Eq. (4)
ω	vorticity
ψ	stream function

Subscripts

e, w, n, s	refer to east, west, north, and south of the grid points (i, j), respectively
n	refer to the outward normal to the boundary contour S
x, y	refer to partial derivatives with respect to x and y, respectively
i, j	refer to grid locations in x- and y-directions, respectively

Acknowledgment

This work was sponsored by Naval Sea Systems Command.

REFERENCES

1. P. J. ROACHE, *Computational Fluid Dynamics* (Hermosa, Albuquerque, NM, 1976), p. 180.
2. S. .G. RUBIN, "Incompressible Navier–Stokes and Parabolized Navier–Stokes Solution Procedures and Computational Techniques," Report, Department of Aerospace Engineering, University of Cincinnati, Cincinnati, OH, 1982 (unpublished).
3. J. E. HARRIS, "Numerical Studies of Incompressible Viscous Flow in a Driven Cavity," NASA SP-378, 1975.
4. W. R. BRILEY, *J. Comput. Phys.* **14**, 8 (1974).
5. K. MIYAKODA, *Japan. J. Geophys.* **3**, 75 (1962).
6. B. J. ALFRINK, in "Proceedings of the Second International Conference on Numerical Methods in Laminar and Turbulent Flow, Venice, 13–16 July, 1981," edited by C. Taylor and B. A. Schrefler (Pineridge Press, Swansea, UK, 1981), p. 75.
7. O. R. BURGGRAF, *J. Fluid Mech.* **24**, 113 (1966).